



Simplified Design of Quad-Band Terahertz Absorber Based on Periodic Closed-Ring Resonator

Pengcheng Lou^{1,2} · Ben-Xin Wang¹ · Yuanhao He¹ · Chao Tang¹ · Qingshan Niu¹ · Fuwei Pi²

Received: 26 December 2019 / Accepted: 5 May 2020 / Published online: 23 May 2020
© Springer Science+Business Media, LLC, part of Springer Nature 2020

Abstract

Multiple-band metamaterial absorbers as an important branch of metamaterial-based resonant devices have shown considerable application prospects in real life. However, current designs have many shortcomings in the realization of multiple-band absorption, including complex pattern structure, time-consuming fabrication steps, and strong interaction between sub-elements. Herein, a simple design of multiple-band metamaterial absorber based on single metallic resonator is presented. Basic cell of the multiple-band absorption is formed by a square metallic patch (cut by a concentric air gap) placed on a metallic mirror separated by an insulating medium material. The metamaterial structure can interact strongly with the incident beam to produce the fundamental mode resonance, third-order resonance, and two other resonances resulted from the concentric air gap introduction. The combining effect of the four discrete resonance modes provides the ability to achieve quad-band absorption. The quad-band absorption shows great dependence on the structure dimensions. Based on this, we further design a kind of multiple-band absorption having the adjustable number of absorption peaks by introducing photosensitive silicon material in the initial area of the air gap. The number of resonance peaks can be tuned flexibly from quad-band absorption to dual-band absorption by changing the conductivity (i.e., material property) of photosensitive silicon material.

Keywords Terahertz metamaterial · Perfect absorber · Quad-band absorption · Closed-ring resonator

Introduction

Metamaterial perfect light absorbers as one of the most exciting topics have attracted much attention because of its important uses [1]. Since the metamaterial perfect light absorbers were first demonstrated in 2008 [2], many types of metamaterial absorption devices have been suggested to meet different application requirements [3–6]. For example, single cross-shaped structure can be used to realize single-band absorption performance [7]. Dual-band/triple-band polarization insensitive metamaterial absorber was presented by using different-sized square metallic patches [8]. Many other shapes of structures, such as split-ring resonator [3], elliptical

resonator [4], spiral resonator [5], and closed-ring resonator [6], have been suggested to meet different application requirements. Among these structures, closed-ring resonator has attracted special research interest due to its simple resonance structure. In view of this, closed-ring resonator-based metamaterial absorbers have been widely suggested [6, 9–19]. Through combing and analyzing a large number of references, it is found that closed-ring resonator-based metamaterial absorption devices mainly focus on multiple-band absorption, i.e., the multiple-band metamaterial absorbers.

However, these multiple-band metamaterial absorbers using closed-ring resonators have many common features [6, 9–19]. Firstly, each closed-ring resonator in these multiple-band metamaterial absorbers typically exhibits single absorption peak caused by the localized resonance response of the closed-ring resonator itself; the superposition effect of multiple localized resonance responses having different frequencies results in the multiple-band absorption. As a result, the basic cell of the multiple-band absorption absorbers exhibits a considerable number of closed-ring resonators having different dimensions. These closed-ring resonators will inevitably have strong interaction, which leads to the degradation of the

✉ Ben-Xin Wang
wangbenxin@hnu.edu.cn

✉ Fuwei Pi
pifuwei@jiangnan.edu.cn

¹ School of Science, Jiangnan University, Wuxi 214122, China

² State Key Laboratory of Food Science and Technology, School of Food Science and Technology, Jiangnan University, Wuxi 214122, China

overall absorption performance of the multiple-band metamaterial absorbers. Secondly, so many closed-ring resonators are usually arranged in two common ways in the basic cell, which are, respectively, the coplanar and stacked. However, the coplanar arrangement has the shortcomings of large cell size (not in line with the current trend of compact design) and strong interaction between these closed-ring resonators (resulting in low absorbance). Accurate alignment between layers and time-consuming fabrication steps are the obstacles that stacked design strategy cannot overcome. It is urgent to design new kind of multiple-band metamaterial absorbers having compact structure, as few resonators as possible and high absorption intensity.

In this paper, a new type of quad-band absorption device based on simple design of metamaterial structure is demonstrated. Its basic cell is formed by a square metallic patch cut by a concentric air gap and an insulating medium material placed on a metallic ground plane having the thickness larger than the skin depth of the incident beam. The designed structure can have strong interaction with the incident beam, resulting in four discrete absorption peaks. The mechanism of the quad-band absorption is investigated; it is revealed that surface metallic structure respectively possesses the fundamental mode resonance response, third-order resonance response, and two new resonance responses resulted from the introduction of the concentric air gap in the square metallic patch; and the combination of these four resonance responses results in the quad-band absorption. Results further show that the resonance performance of quad-band absorption device exhibits large dependence on the surface metallic structure, including the square patch length and the introduced air gap length, which have a considerable degree of freedom to design the metamaterial absorber with specific structure dimensions according to different application needs.

Compared with the current design strategies to gain the multiple-band absorption, the results obtained here should have the following advantages. Firstly, the multiple-band absorption device only uses one metallic surface structure, which is obviously superior to the existing multiple-band metamaterial absorbers that the number of metallic resonators is typically greater than (or at least equal to) the resonance peaks of the multiple-band absorption [6, 9–19]. This suggests that it can simplify the surface structure design of the multiple-band metamaterial absorbers. Secondly, the utilization of the single metallic resonator should have the smaller cell dimension over previous designs, which is in line with the current trend of compact structure design and therefore provides the possibility to simplify the fabrication processes of the metamaterial absorption devices. Thirdly, the underlying physical origin of the quad-band absorption is derived from the combination of the fundamental mode resonance response, third-order resonance response, and other two new resonance responses in the surface metallic resonator, which is obviously

different from the previous designs that only employ the single resonance response of the metallic element. From this point of view, the design proposed here can expand or enrich the working mechanism of existing multiple-band metamaterial absorbers to a certain extent. In addition, considering the different working mechanism, the influence of structure dimensions on the absorption performance is also different.

Materials and Design

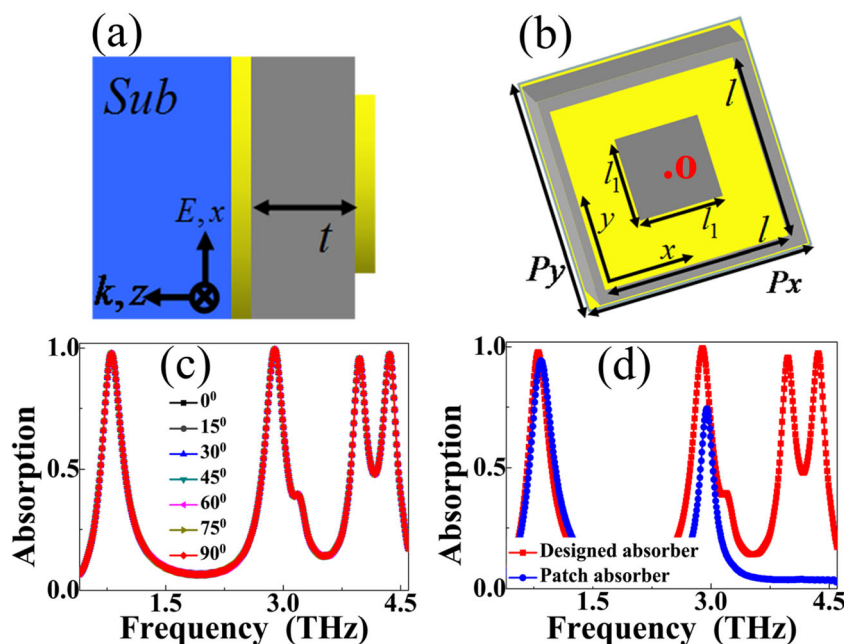
The schematic of the quad-band metamaterial absorption device is consisted of only a patterned metallic array and an insulating medium material on top of a metallic board having the thickness larger than the skin depth of the incident beam (see Fig. 1a and b). The upper and lower metallic layers are both constructed by the gold (Au) with the fixed conductivity of 4.09×10^7 S/m. The insulating medium material between the upper and lower metallic layers is polyimide, which has a thickness of $t = 15 \mu\text{m}$ and dielectric constant of $1.733 + i0.06$. The lossy intermediate material plays the rather important role in achieving the perfect absorption at terahertz or longer wavelengths [1].

The surface (or top) structure of the basic cell actually is a square metallic patch cut by a concentric air gap. The length and width of the square metallic patch are both $l = 60 \mu\text{m}$. The introduced concentric air gap into the square metallic patch has the same dimensions of the length and width, which are both $l_1 = 26 \mu\text{m}$. According to this, the line-width of the surface metallic structure is $(l - l_1)/2 = 17 \mu\text{m}$, which is larger than that the common metallic resonators [6, 9–19]. Of course, the ratio of line-width to resonator length is also larger than that of common metallic resonators in [6, 9–19]. It is found that large line-width is the key to achieve quad-band absorption response.

The basic cell is periodically arranged in the directions of x - and y -axis having the dimensions of $P = P_x = P_y = 65 \mu\text{m}$. In order to achieve the expected results, commercial numerical simulation software (FDTD Solutions 8.6-version) is adopted to solve the Maxwell equations based on the finite-difference time-domain method. A plane electromagnetic wave vertically irradiates the designed metamaterial structure along the position direction of the z -axis (from the surface metallic structure to the bottom metallic board). Periodic boundary conditions are applied in both directions of x - and y -axis; perfectly matching layers are employed along the z -axis (or the incident beam propagation direction).

The absorption of the designed metamaterial structure is expressed by $A = 1 - T - R$, of which the A is the absorption rate and T and R are, respectively, the rates of transmission and reflection. We can get the perfect absorption when the T and R are both suppressed (or equal to zero). The transmission T is

Fig. 1 **a** Side view and **b** top view of the quad-band metamaterial absorber. **c** Absorption spectra of the designed quad-band metamaterial absorber under different angles of polarization. **d** Comparative absorption spectra of quad-band metamaterial absorber (with red curve) and patch absorber (with blue curve). The origin of coordinate, which is actually the center of the top metallic array of the lattice structure (marked with red o in (b))



actually equal to zero because of the existing of the bottom metallic board, where its thickness is larger than the incident beam skin depth. The reflection R can also be optimized to zero by tuning the thickness of insulating medium material, i.e., the impedance of the metamaterial structure [20–27].

Results and Discussion

Figure 1c gives the absorption of the designed device. Four large absorption rates (in an average of 97.54%) of discrete peaks are realized. The frequencies of them are, respectively, 0.80 THz, 2.89 THz, 3.98 THz, and 4.36 THz. For illustration, the four bands are named as B1, B2, B3, and B4, respectively.

Unlike the works in Table 1 that single metallic resonator corresponds to at most one absorption peak, we obtain quad-band absorption through only utilizing one patterned metallic array. The structure presented here should have many merits, including the simplification of the structure design, rapid construction processes, and novel physical mechanism, over the works in Table 1. Additionally, because the patterned metallic array has the feature of high degree of symmetry, the device is insensitive to the angles of polarization (see Fig. 1c).

In order to preliminary investigate the origin of the B1, B2, B3, and B4, one additional device (called patch absorber), consisted of square gold patch and insulating intermediate layer on top of gold board, is introduced. Besides without the air gap, the parameters of patch absorber are same to that

Table 1 Comparisons of performances among designs in previous works

Reference	Absorption peaks	Obtained methods: coplanar (C), stacked (S)	Number of elements
9	1	S	2
10	2	C	2
11	2	C + S	8
12	2	C	4
13	2	C	4
14	2	C	2
15	3	C	3
16	3	C	3
17	3	C	9
18	3	C	8
19	3	C	3
20	4	C + S	4
This paper	4	—	1

of the presented quad-band absorption device. The absorption of the patch absorber is shown in the blue curve of Fig. 1d. There are two distinct bands at frequencies of 0.84 THz and 2.94 THz, and the frequencies of them are very close to that of the B1 and B2 (see Fig. 1d), which indicate that the mechanisms of B1 and B2 should be consistent with the dual-band absorption in patch absorber. We also observed that the introduction of the air gap (i.e., the closed-ring resonator) brings two new bands, that is, B3 and B4. Further results demonstrate that the performance of B3 and B4 can be controlled via the air gap sizes (see below Fig. 4a and b).

Figure 2a to d provide the field ($|E|$ and $|Hy|$) distributions of the two modes of patch absorber. The $|E|$ fields of them in Fig. 2a and c are very similar and are both distributed in both edges of the Au patch. However, obvious differences can be found for the $|Hy|$. The only one distribution region in Fig. 2b is observed for the first mode of the patch absorber, while three regions are seen in Fig. 2d for the second mode. The $|Hy|$ distributions prove that the first and the second modes are, respectively, originated from first-order and third-order resonances of the patch absorber. Furthermore, the $|E|$ and $|Hy|$ of B1 and B2 in Fig. 2e–h are very similar to that of patch absorber in Fig. 2a–d, which means that the mechanisms of B1 and B2 are, respectively, the first-order and third-order resonances of the patterned surface structure (or closed-ring resonator). Moreover, by comparison with Fig. 2, the $|E|$ and $|Hy|$ in B3 and B4 and in B1 and B2 are apparently different. The $|E|$ fields in Fig. 3a and d not only focus on both edges of the patterned surface structure but also both edges of the air gap. The aggregation intensity of them in both edges of the air gap is greater than that of the edges of the patterned surface structure, while the $|E|$ fields in both edges of the air gap are smaller than that of both edges of the patterned surface

structure (see Fig. 2e and g). That is to say, the introduction of air gap plays an emphasis role in the formation of B3 and B4.

Although at first glance the $|E|$ distributions of B3 and B4 are very similar, the essence of them is different, which can refer to the real Ez and the $|Hy|$. The real Ez in Fig. 3b shows that the charge distributions of B3 are mainly concentrated on the middle region of the edges of the patterned surface structure and both edges of the air gap. However, for B4, as seen in Fig. 3e, its charges are basically gathered in 4 corners of the edges of the patterned surface structure and both edges of the air gap. The $|Hy|$ fields of the two modes in Fig. 3c and f also show completely different distribution features. By comparing the field distributions of the two modes, the mechanisms of B3 and B4 should be caused by two different cavity resonances. The combination of the first-order and third-order responses of the patterned surface structure and two additional modes caused by the air gap result in the quad-band absorption.

Because B3 and B4 are determined by the air gap, its size (l_1) change will inevitably influence the performance of the two modes. As shown in Fig. 4a, the last two modes gradually disappear with the l_1 decrease, while the B1 and B2 are nearly unchanged. As a result, we just obtain a dual-band absorption when l_1 is less than 14 μm . When the l_1 is increased, as seen in Fig. 4b, we found that not only the B3 and B4 but also the B1 and B2 are also strongly affected. These results prove that we can employ different l_1 to tune the performance of the device, in particular of the performance of B3 and B4. The changes in the first two modes should be due to the variations in their effective length because of the increase of the l_1 .

The four absorption peaks can also be controlled by other parameters. As shown in Fig. 4c, the resonance frequencies of the four absorption peaks exhibit the similar change trends

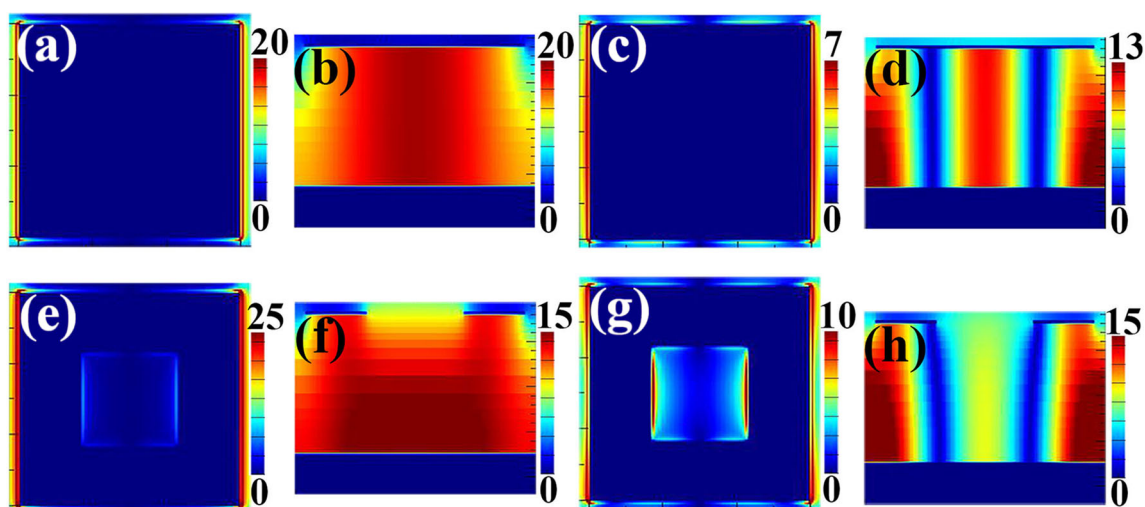
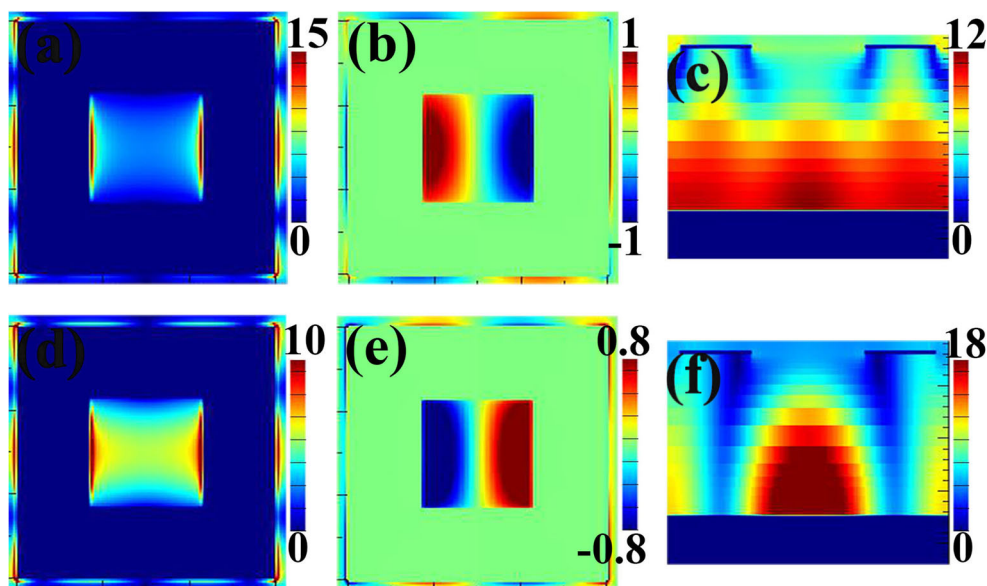


Fig. 2. a and b are, respectively, the $|E|$ and $|Hy|$ of the first peak of patch absorber; c and d are, respectively, the $|E|$ and $|Hy|$ of the second peak of patch absorber; e and f are respectively the $|E|$ and $|Hy|$ of the mode B1 of

quad-band metamaterial absorber; and g and g are respectively the $|E|$ and $|Hy|$ of the mode B2 of quad-band metamaterial absorber

Fig. 3 **a**, **b**, and **c** are, respectively, the $|E|$, real E_z , and $|Hy|$ of the mode B3 of quad-band metamaterial absorber. **d**, **e**, and **f** are, respectively, the $|E|$, real E_z , and $|Hy|$ of the mode B4 of quad-band metamaterial absorber



that gradually decrease with the increase of the length (l) of the patterned surface structure. This kind of change trend shows that the longer the length (l) is, the smaller the resonance frequencies are. This is consistent with previous theoretical demonstration that the resonance frequency of the patterned metallic resonator is mainly inversely proportional to the length of the patterned resonator itself [1]. However, different from the length change of the air gap in Fig. 4a and b, the variation of the length (l) does not affect the number of the absorption peaks; that is, there is no case that the absorbance of one or some specific resonance peaks is suppressed. In addition, we observed in Fig. 4d that the resonance frequencies of the four absorption peaks also show obvious

dependence on the thickness (t) of the insulating medium layer. It should be noted that when the thickness of the insulating medium layer is equal to $19\ \mu\text{m}$, the last absorption peak B4 can be nearly suppressed, thus showing the triple-band absorption performance.

Potential Application

The potential application of the quad-band metamaterial absorption device is discussed in this section. Here it can be designed as an adjustable absorption device by introducing photosensitive silicon material into the initial air gap (i.e., the initial air gap is replaced by the photosensitive silicon

Fig. 4 Dependence of the absorption on the size changes of the air gap in ranges of $8\ \mu\text{m}$ to $26\ \mu\text{m}$ (**a**) and $26\ \mu\text{m}$ to $50\ \mu\text{m}$ (**b**). Dependence of the absorption on the length (l) changes of the patterned surface structure (**c**), thickness (t) changes of the insulating dielectric layer (**d**)

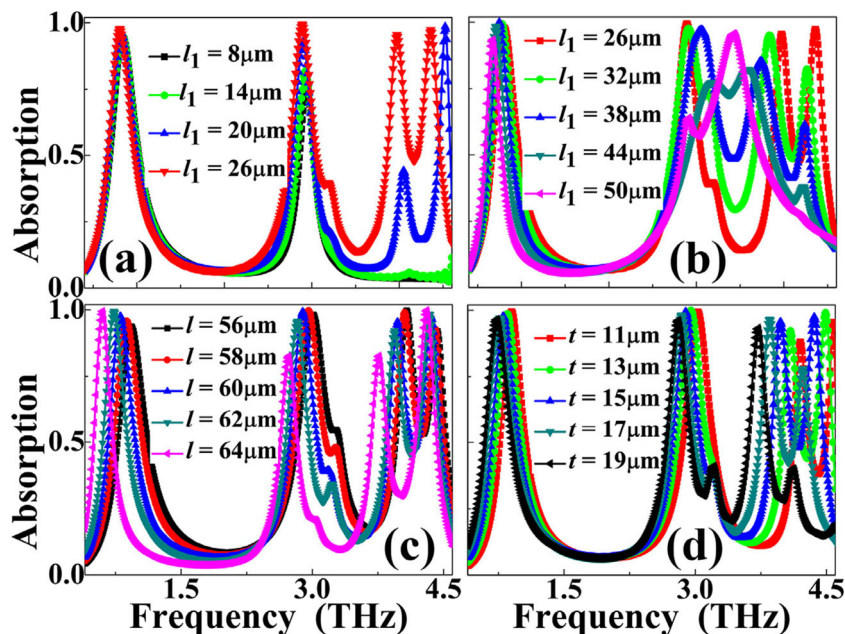
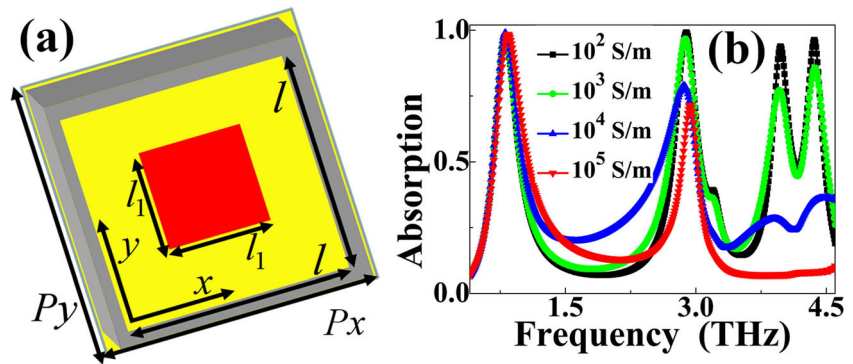


Fig. 5 **a** Structure diagram of the tunable metamaterial absorption device. **b** Absorption spectra of the tunable metamaterial absorption device under different photosensitive silicon conductivity



material). Figure 5a gives the top view of the tunable metamaterial absorption device. The red area stands for the photosensitive silicon material, while other geometrical parameters are all unchanged (or consistent with the above section). As we all know, photosensitive silicon material can regulate its own conductivity through external stimulation, thus realizing the conversion from the dielectric to metallic [28, 29]. The larger the conductivity, the more obvious the metallic property [28, 29].

When the conductivity of photosensitive material is low (less than 1000 S/m), it can show dielectric property [28, 29]. Because the air is a kind of special dielectric material, the photosensitive silicon material with low conductivity should show quad-band absorption response. As shown in the black curve of the Fig. 5b, the designed multiple-band absorption device having the photosensitive silicon material conductivity of 100 S/m indeed possesses four absorption peaks. However, the absorbance of the last three absorption peaks (especially the last two absorption peaks) shows a decreasing trend when the conductivity of the photosensitive silicon material is increased. This is mainly due to the property change of the photosensitive silicon material.

The photosensitive silicon material having the conductivity of 100,000 S/m can present the metallic property [28, 29]. The combination of the metallic property of the photosensitive silicon material with the outer metallic section (or the outer closed ring) can be considered to form a complete square metallic patch. The absorption response of the square metallic patch has been discussed in the above section, which can achieve the dual-band absorption (see the blue curve in Fig. 1d). It can be predicted that when the photosensitive silicon has high conductivity (or exhibits the metallic property), there should be two absorption peaks on its resonance curve. As observed in the red curve of the Fig. 5 b, two absorption bands (or dual-band absorption) are indeed gained when the conductivity of the photosensitive silicon is 100,000 S/m, which is consistent with the theoretical prediction. Based on these results, we can see clearly that the design of the multiple-band absorption device has the ability to tune the number of absorption peaks (from the quad-band absorption to the dual-

band absorption) by changing the external stimulus to cause the conversion of photosensitive silicon from the dielectric to metallic property. It also reflects that the designed multiple-band absorption device has the characteristics of switching, which could find important application prospects in real life [30], such as sample detection and refractive index sensing.

Conclusion

In conclusion, quad-band metamaterial absorber operated at terahertz domain using simple design of surface structure is demonstrated. The surface structure is a square metallic patch cut by a concentric air gap. The surface structure placed on a continuous metallic board separated by an insulating medium layer forms the basic cell of the quad-band absorption. The basic cell of metamaterial structure can resonate strongly with the incident terahertz wave, resulting in fundamental mode response, third-order response, and two other resonances induced by the introduced concentric air gap. The superposition of the four discrete resonance responses generates four absorption peaks at once. The corresponding field distribution of each absorption peak is provided to reveal the underlying physical mechanism of the quad-band absorption. The quad-band absorption has great dependence on the air gap length, square patch length, and insulating medium layer thickness. Compared with existing works using many different-sized metallic resonators to achieve multiple-band absorption, the strategy presented here can significantly reduce the number of the metallic elements, simplify the structure design, and save fabrication time and cost, and therefore many potential applications could be found. As a typical example, we present an adjustable metamaterial absorber using photosensitive silicon replaced the initial air gap. The photosensitive silicon has the variable conductivity (or variable material properties from dielectric to metallic) through external stimulation. Results show that the designed metamaterial absorber can be adjusted from the quad-band absorption to dual-band absorption by gradually increasing the conductivity of the photosensitive

silicon (or the photosensitive silicon transits from the properties of the dielectric to metallic).

Funding Information This research was funded by the National Natural Science Foundation of China (21603087, 11647143), the Natural Science Foundation of Jiangsu (BK20160178, BK20160189), the China Postdoctoral Science Foundation (2019 M651692), the Jiangsu Postdoctoral Science Foundation (2018K113C), and the Fundamental Research Funds for Central Universities (JUSRP51721B).

References

- Watts CM, Liu X, Padilla WJ (2012) Metamaterial Electromagnetic Wave Absorbers. *Adv Mater* 24:OP98. <https://doi.org/10.1002/adma.201200674>
- Landy NI, Sajuyigbe S, Mock JJ, Smith DR, Padilla WJ (2008) Perfect metamaterial absorber. *Phys Rev Lett* 100:207402
- Wu PC, Liao CY, Chen JW, Tsai DP (2017) Isotropic absorption and sensor of vertical split-ring resonator. *Adv Opt Mater* 5:1600581
- Yao G, Ling F, Yue J, Luo C, Ji J, Yao J (2016) Dual-band tunable perfect metamaterial absorber in the THz range. *Opt Express* 24:1518–1527
- Wang W, Yan M, Pang Y, Wang J, Ma H, Qua S, Chen H, Xu C, Feng M (2015) Ultra-thin quadri-band metamaterial absorber based on spiral structure. *Appl Phys A Mater Sci Process* 118:443–447
- Kim JH, Hokmabadi MP, Balci S, Rivera E, Wilbert D, Kung P, Kim SM (2016) Investigation of robust flexible conformal THz perfect metamaterial absorber. *Appl Phys A Mater Sci Process* 122:362
- Chen HT (2012) Interference theory of metamaterial perfect absorbers. *Opt Express* 20:7165–7172
- Zhang B, Hendrickson J, Guo J (2013) Multispectral near-perfect metamaterial absorbers using spatially multiplexed plasmon resonance metal square structures. *J Opt Soc Am B* 30:656
- Ma Y, Chen Q, Grant J, Saha SC, Khalid A, Cumming DRS (2011) A terahertz polarization insensitive dual band metamaterial absorber. *Opt Lett* 36:945–947
- Bhattacharyya S, Ghosh S, Chaurasuya D, Srivastava KV (2015) Bandwidth-enhanced dual-band dual-layer polarization-independent ultra-thin metamaterial absorber. *Appl Phys A Mater Sci Process* 118:207–215
- Zhong J, Huang Y, Wen G, Sun H, Wang P, Gordon O (2012) Single-/dual-band metamaterial absorber based on cross-circular-loop resonator with shorted stubs. *Appl Phys A Mater Sci Process* 108:329–335
- Bhattacharyya S, Srivastava KV (2014) *J Appl Phys* 115:104503
- Ayop O, Rahim MKA, Murad NA, Samsuri NA (2016) Dual-resonant polarization-independent and wide-angle metamaterial absorber in X-band frequency. *Appl Phys A Mater Sci Process* 122:374
- Shen X, Cui TJ, Zhao J, Ma HF, Jiang WX, Li H (2011) Polarization-independent wide-angle triple-band metamaterial absorber. *Opt Express* 19:9401–9407
- Shen X, Yang Y, Zang Y, Gu J, Han J, Zhang W, Cui TJ (2012) Triple-band terahertz metamaterial absorber: design, experiment, and physical interpretation. *Appl Phys Lett* 101:154102
- Park JW, Tuong PV, Rhee JY, Kim KW, Jang WH, Choi EH, Chen LY, Lee YP (2013) Multi-band metamaterial absorber based on the arrangement of donut-type resonators. *Opt Express* 21:9691
- Bhattacharyya S, Ghosh S, Srivastava KV (2013) Triple band polarization-independent metamaterial absorber with bandwidth enhancement at X-band. *J Appl Phys* 114:094514
- Bhattacharyya S, Ghosh S, Srivastava KV (2014) Equivalent circuit model of an ultra-thin polarization-independent triple band metamaterial absorber. *AIP Adv* 4:097127
- Liu S, Zhuge J, Ma S, Chen H, Bao D, He Q, Zhou L, Cui TJ (2015) A bi-layered quad-band metamaterial absorber at terahertz frequencies. *J Appl Phys* 118:245304
- Wang BX, Wang GZ, Wang LL (2016) Design of a novel dual-band terahertz metamaterial absorber. *Plasmonics* 11:523–530
- Wang BX, Wang GZ, Sang T (2016) Simple design of novel triple-band terahertz metamaterial absorber for sensing application. *J Phys D* 49:165307
- Wang BX (2017) Quad-Band Terahertz Metamaterial Absorber Based on the Combining of the Dipole and Quadrupole Resonances of Two SRRs. *IEEE J Select Top Quantum Electron* 23:4700107. <https://doi.org/10.1109/JSTQE.2016.2547325>
- Wang BX, Wang GZ, Huang WQ (2017) Single metamaterial resonator having five-band terahertz near-perfect absorption. *IEEE Photon Technol Lett* 29:1888–1891
- Wang BX, Tang C, Niu Q, He Y, Chen T (2019) Design of narrow discrete distances of dual-/triple-band terahertz metamaterial absorbers. *Nanoscale Res Lett* 14:64
- Wang BX, He Y, Lou P, Xing W (2020) Design of a dual-band terahertz metamaterial absorber using two identical square patches for sensing application. *Nanoscale Adv* 2:763–769
- Wang BX, He Y, Lou P, Huang WQ, Pi F (2020) Penta-band terahertz light absorber using five localized resonance responses of three patterned resonators. *Results Phys* 16:102930
- Wang BX, He Y, Xu N, Wang X, Wang Y, Cao J (2020) Design of dual-band polarization controllable metamaterial absorber at terahertz frequency. *Results Phys* 17:103077
- Shen NH, Kafesaki M, Koschny T, Zhang L, Economou EN, Soukoulis CM (2009) Broadband blueshift tunable metamaterials and dual-band switches. *Phys Rev B* 79:161102
- Chen HT, Ohara JF, Azad AK, Taylor AJ, Averitt RD (2008) Experimental demonstration of frequency-agile terahertz metamaterials. *Nat Photon* 2:295–298
- Chen L, Liao DG, Guo XG, Zhao JY, Zhu YM, Zhuang SL (2019) Terahertz time-domain spectroscopy and micro-cavity components for probing samples: a review. *Front Inform Technol Electron Engine* 20:591–607

Publisher's Note Springer Nature remains neutral with regard to jurisdictional claims in published maps and institutional affiliations.